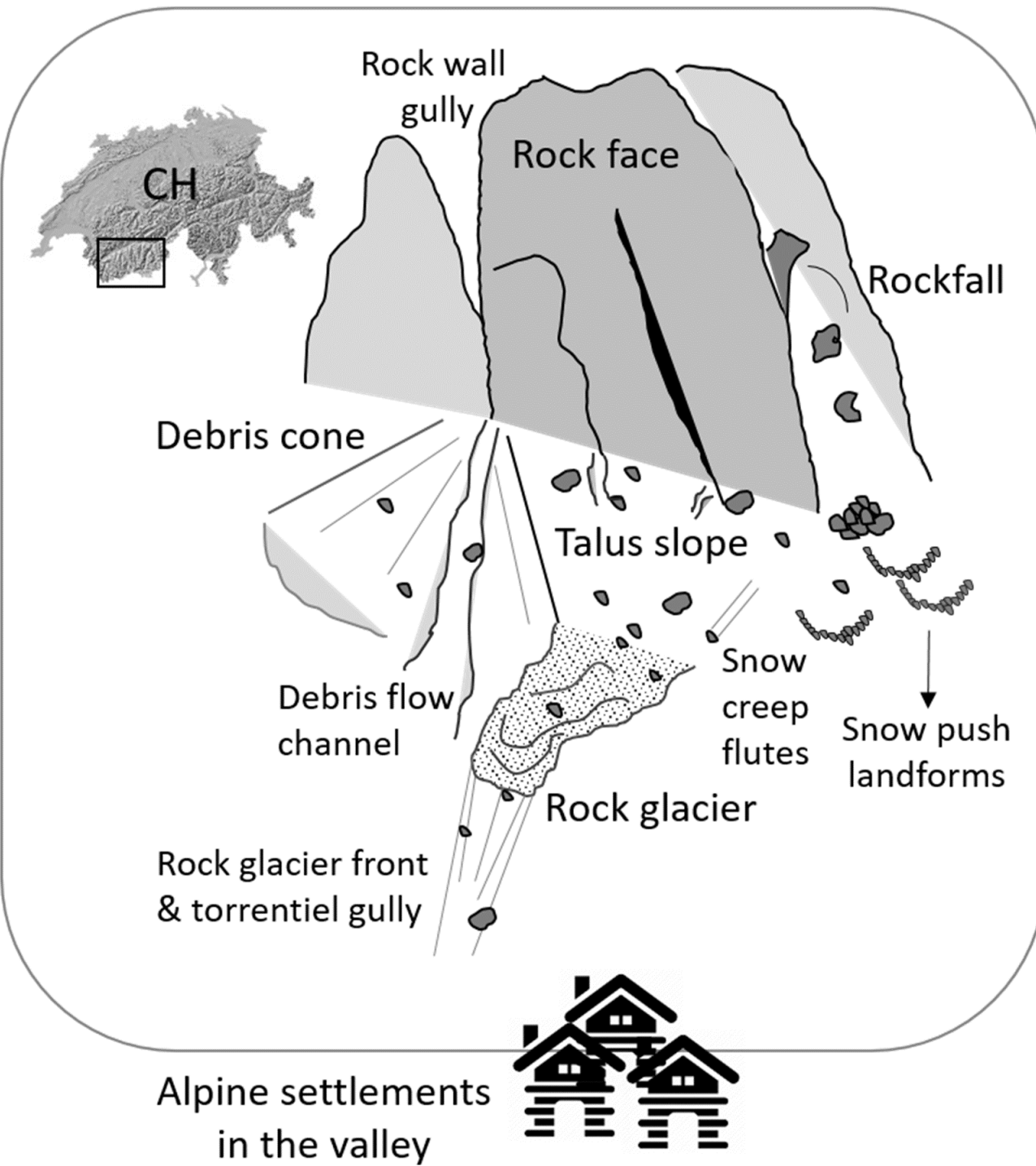


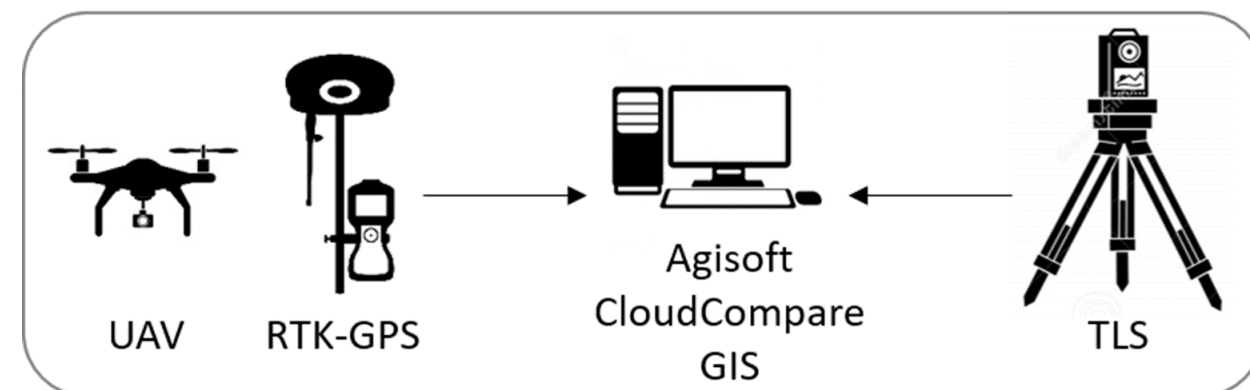
Hanne Hendrickx, Reynald Delaloye, Jan Nyssen, Amaury Frankl

RECENT GEOMORPHIC DESTABILIZATION OF MOUNTAIN SLOPES, A POSSIBLE LINK TO CLIMATE CHANGE? TWO CASE STUDIES FROM SWITZERLAND

a) The study object: geomorphic processes



b) The monitoring tools



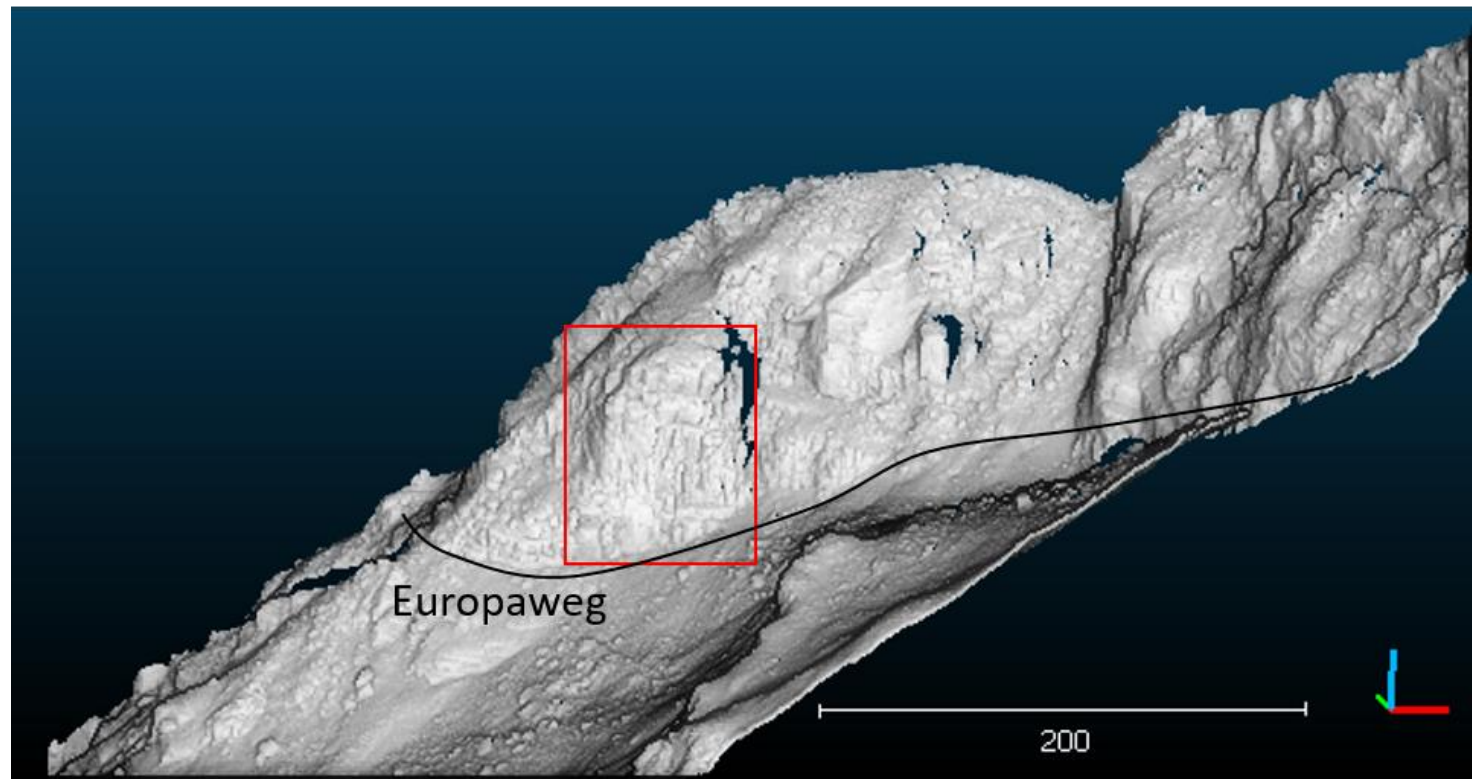
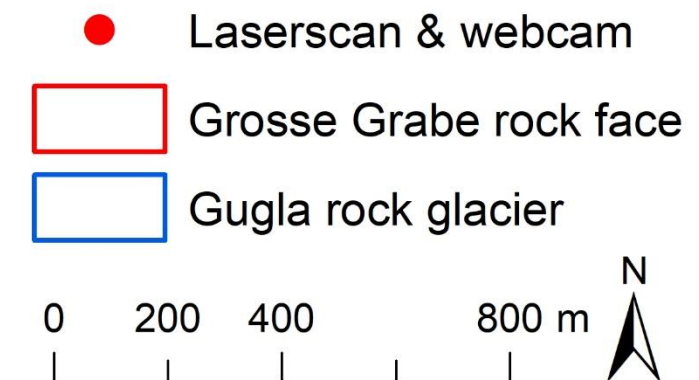
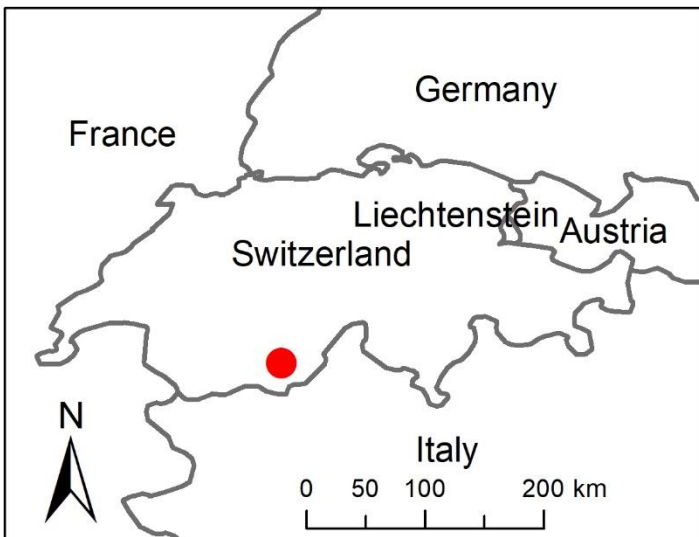
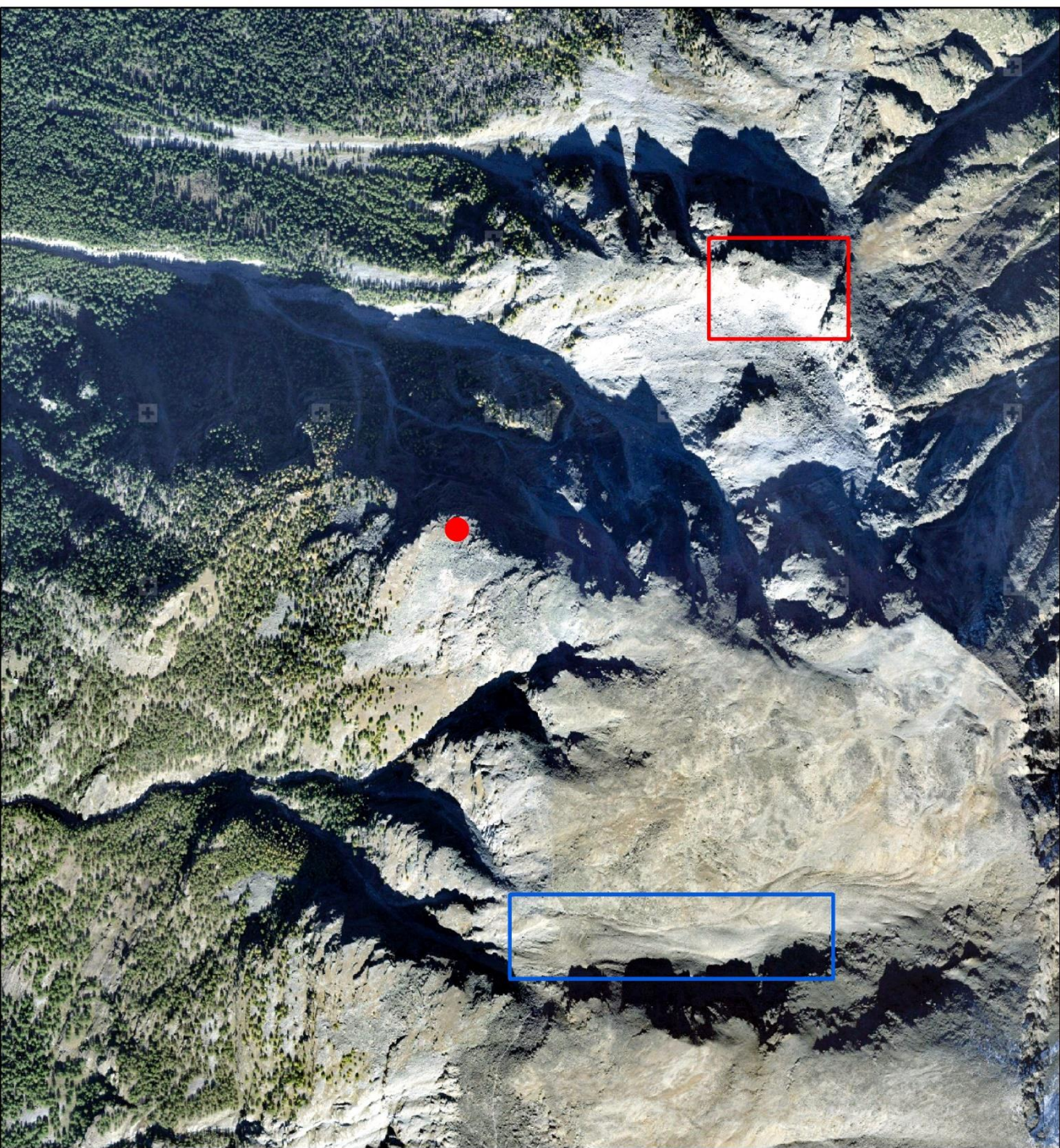
FRAMEWORK OF THIS STUDY

- Geomorphic destabilisations in high mountain areas are often linked to permafrost degradation and changing precipitation intensities, induced by climate change.
- Keeping in mind the complex interaction between meteorological and geological conditions, two alpine mass movements were investigated with regard to their possible causes (2017 – 2019).

Figure 1. a) the studied high alpine environment with the different geomorphic processes observed, b) the used methods for monitoring these landscapes (technical specs at the end of the slides).

CASE STUDY 1

CASE STUDY 1: GROSSE GRABE ROCK FACE



CASE STUDY 1: GROSSE GRABE ROCK FACE

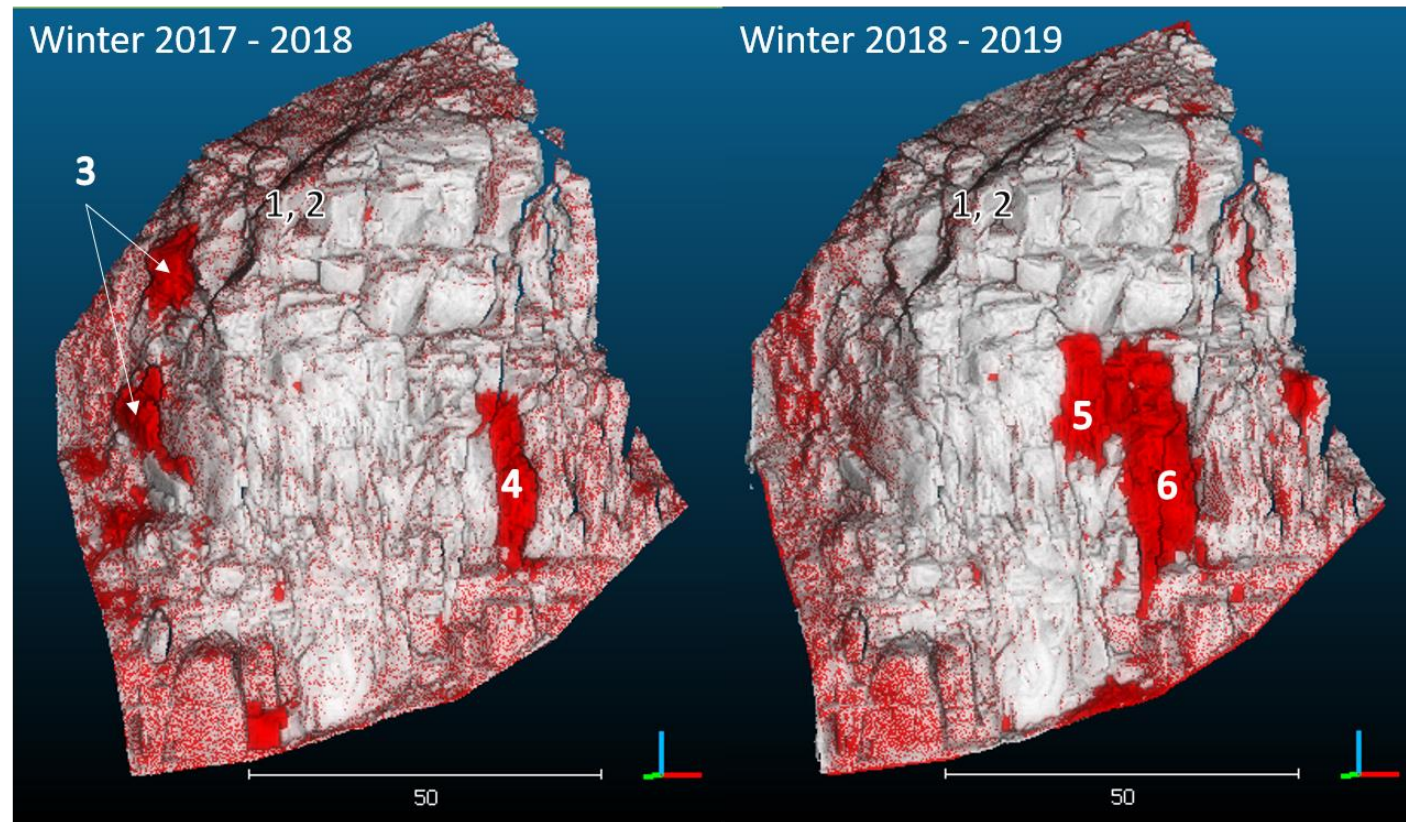


Figure 2. Observed winter rock fall.

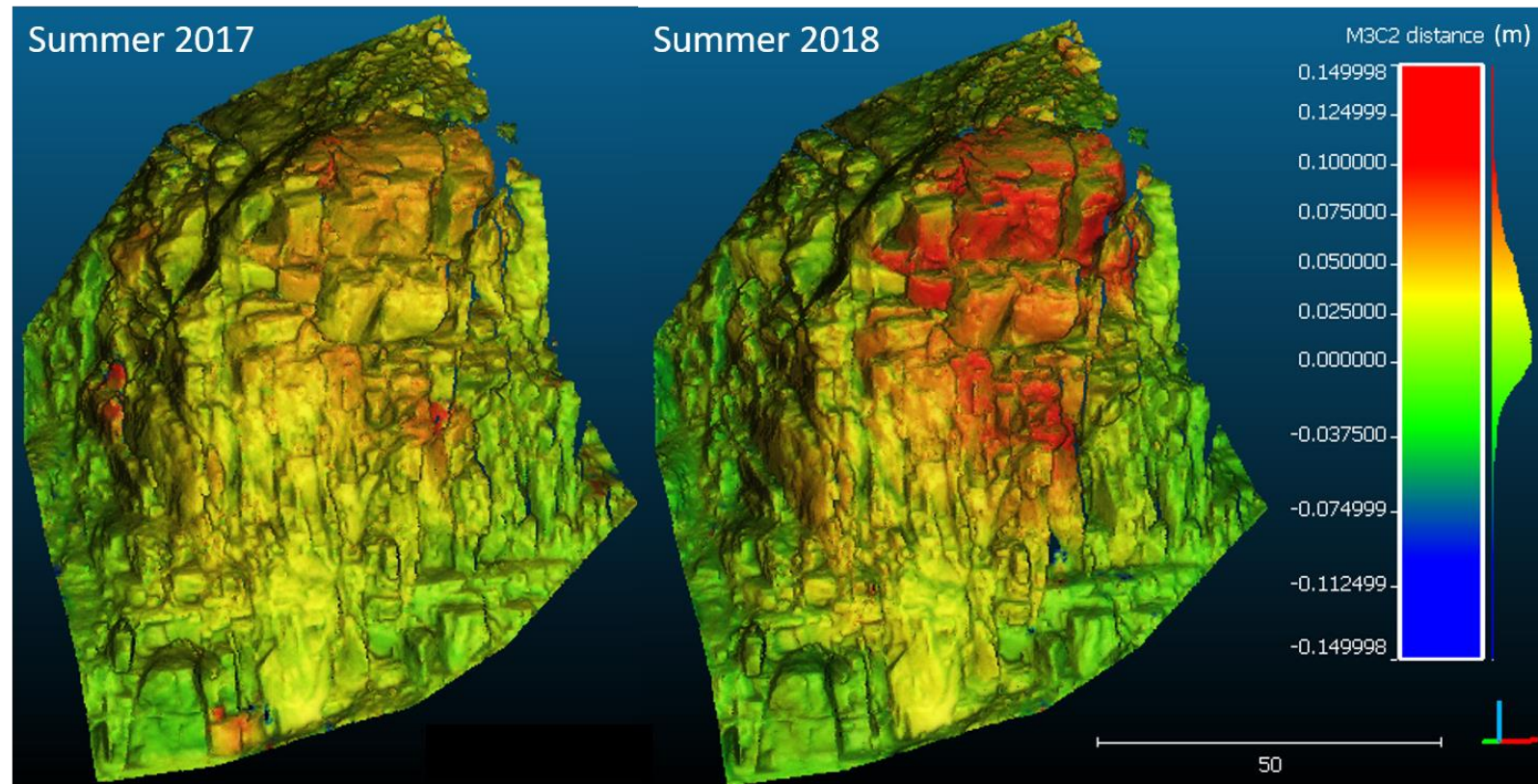


Figure 3. Observed summer deformation.

- Isolated rock fall started in January 2017 (webcam observations) → launching the TLS campaign (Fig. 2).
- The next two summers the rock face had been tilting at an increasing rate: 1 - 3,3 cm/month (Fig. 3).

CASE STUDY 1: GROSSE GRABE ROCK FACE

- Summer 2019, consecutive large rock fall events ($> 10,000 \text{ m}^3$) lead to the complete collapse of the rock face with a total volume of more than $60,000 \text{ m}^3$ (Fig. 4, Fig. 5, Fig. 6).
- The wet rock fall scar probably indicates permafrost thawing (Fig. 6). Besides the geological characteristics, which are favouring the rock wall instability, multi-decennial warming of the permafrost is presumably an implicated factor.

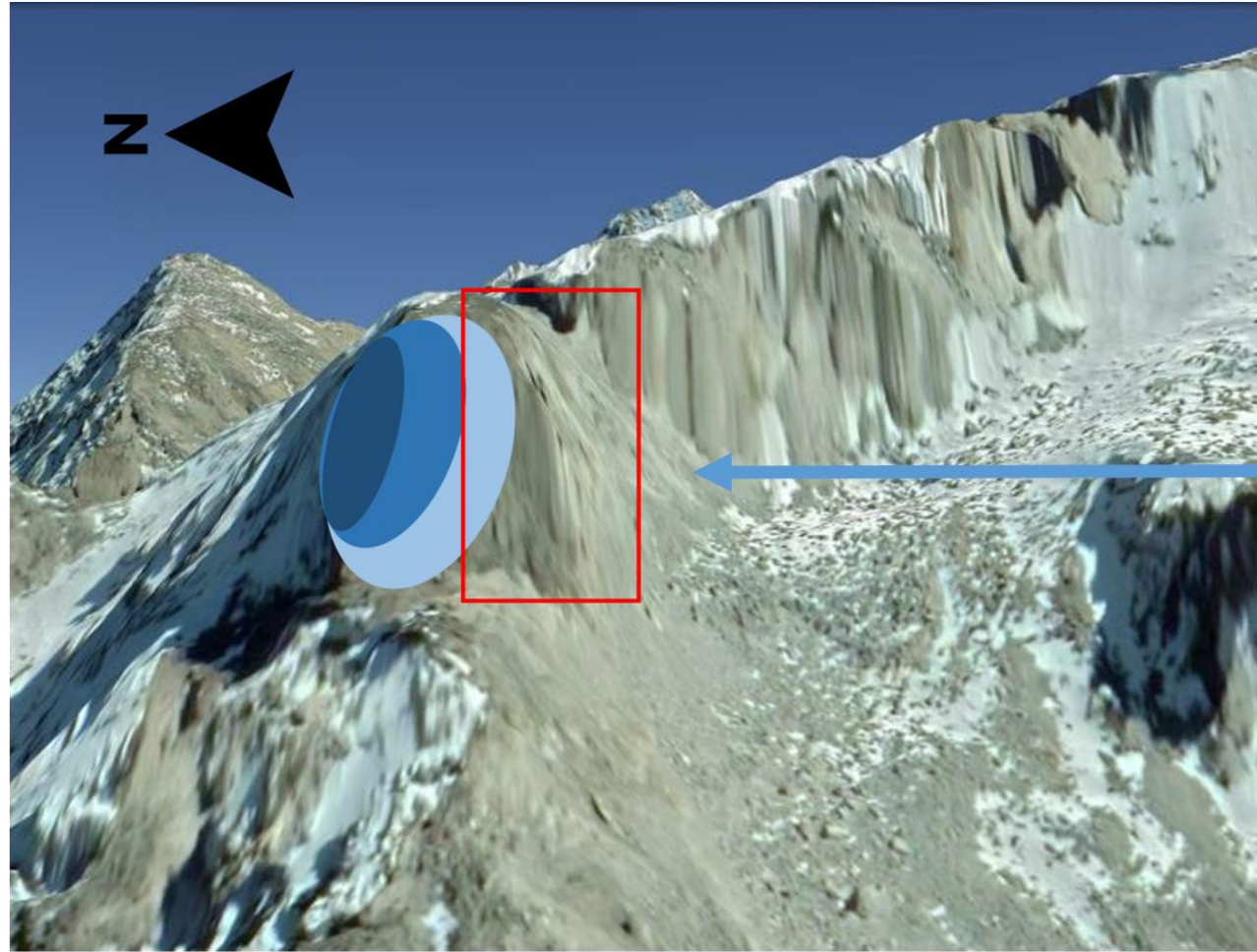
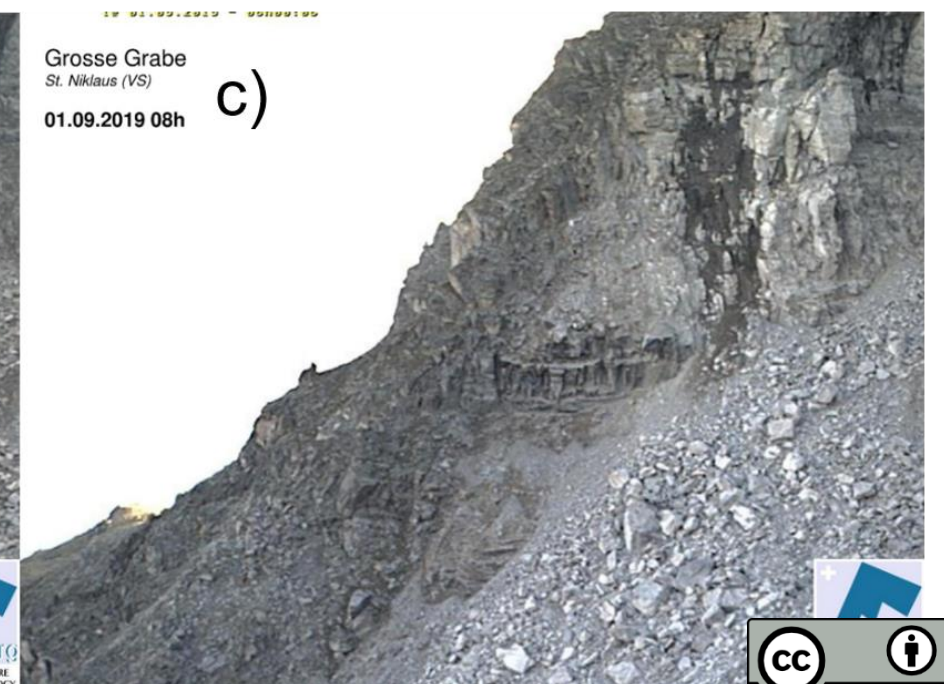
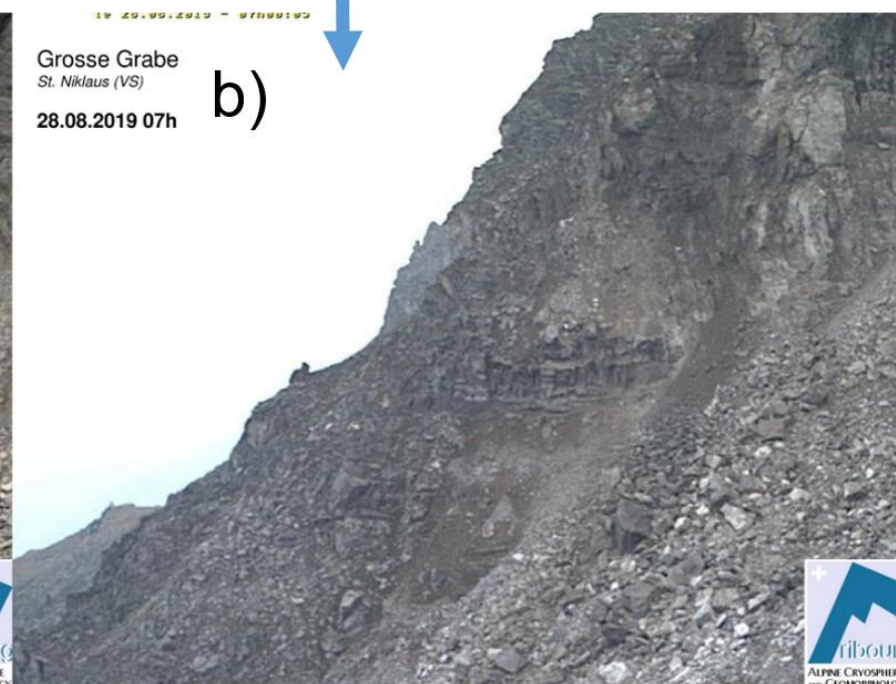


Figure 4. Assumed permafrost setting of the collapsed rock face.

The collapse of the rock face: 63,138 m³ of total volume

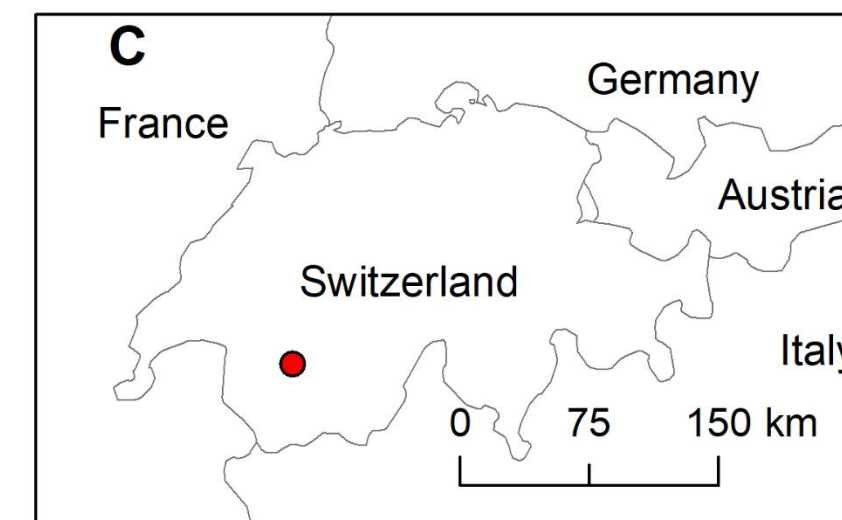
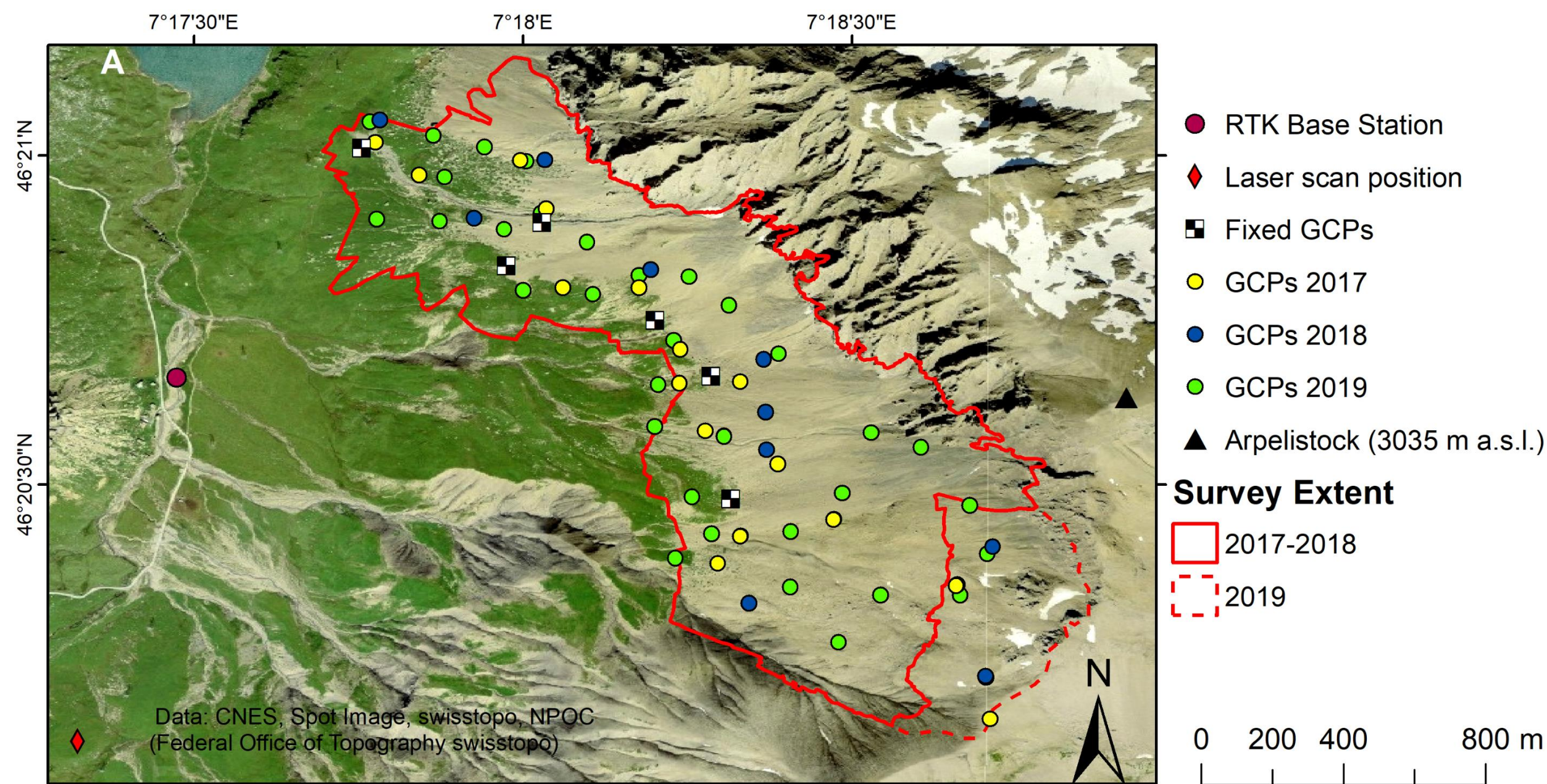
Rock fall dates		Volume in m ³
1	21/01/2017 17h – 22/01/2017 10h (UTC+1)	Est. 500
2	21/05/2017 20-21h (UTC+2)	Est. 500
3	20/05/2018 18h – 21/05/2018 07h (UTC+2)	513
4	30/05/2018 20h – 31/05/2018 07h (UTC+2)	318
5	13/01/2019 13h - 14/01/2019 11h (UTC+1)	346
6	16/04/2019 17h – 17/04/2019 08h (UTC+2)	756
7	15/07/2019 16-17h (UTC+2)	Est. 1000
8	27/08/2019 18h46 (UTC+2)	Est. 15 000
9	28/08/2019 00h10 (UTC+2)	Est. 30 000
10a	02/09/2019 04h53 (UTC+2)	Est. 10 000
10b	02/09/2019 12h49 (UTC+2)	
11a	05/09/2019 06h33 (UTC+2)	Est. 5000
11b	05/09/2019 12h50 (UTC+2)	
12	22/10/2019 13h19 (UTC+2)	Est. 1000 – 2000 ??
13	23/10/2019 13-14h (UTC+2)	Est. 100-500
14	23/10/2019 17h – 24/10/2019 12h (UTC+2) (various)	Est. 50-200
15	27/10/2019 17h – 28/10/2019 10h (UTC+1)	<25
16	30/10/2019 10h – 12h (UTC+1)	<25

Figure 5. Rock fall dates from webcam imagery and volumes from TLS.



CASE STUDY 2*

CASE STUDY 2: COL DU SANETSCH TALUS SLOPE



CASE STUDY 2: COL DU SANETSCH TALUS SLOPE

- General geomorphic processes on the studied talus slope are dominated by debris flow scour and deposits, snow push phenomena (ridges and flutes) and occasional rill erosion (Fig. 8).

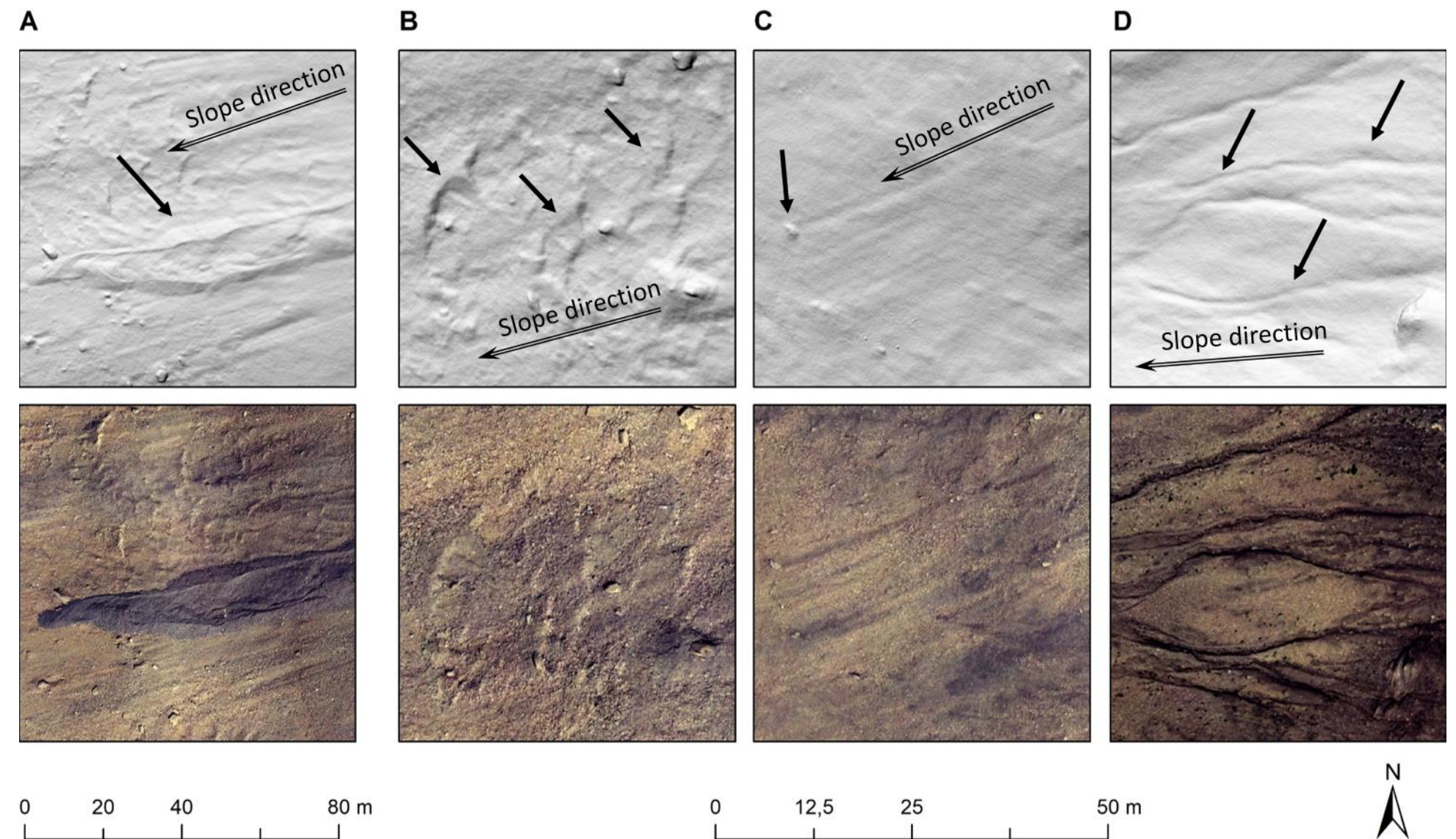
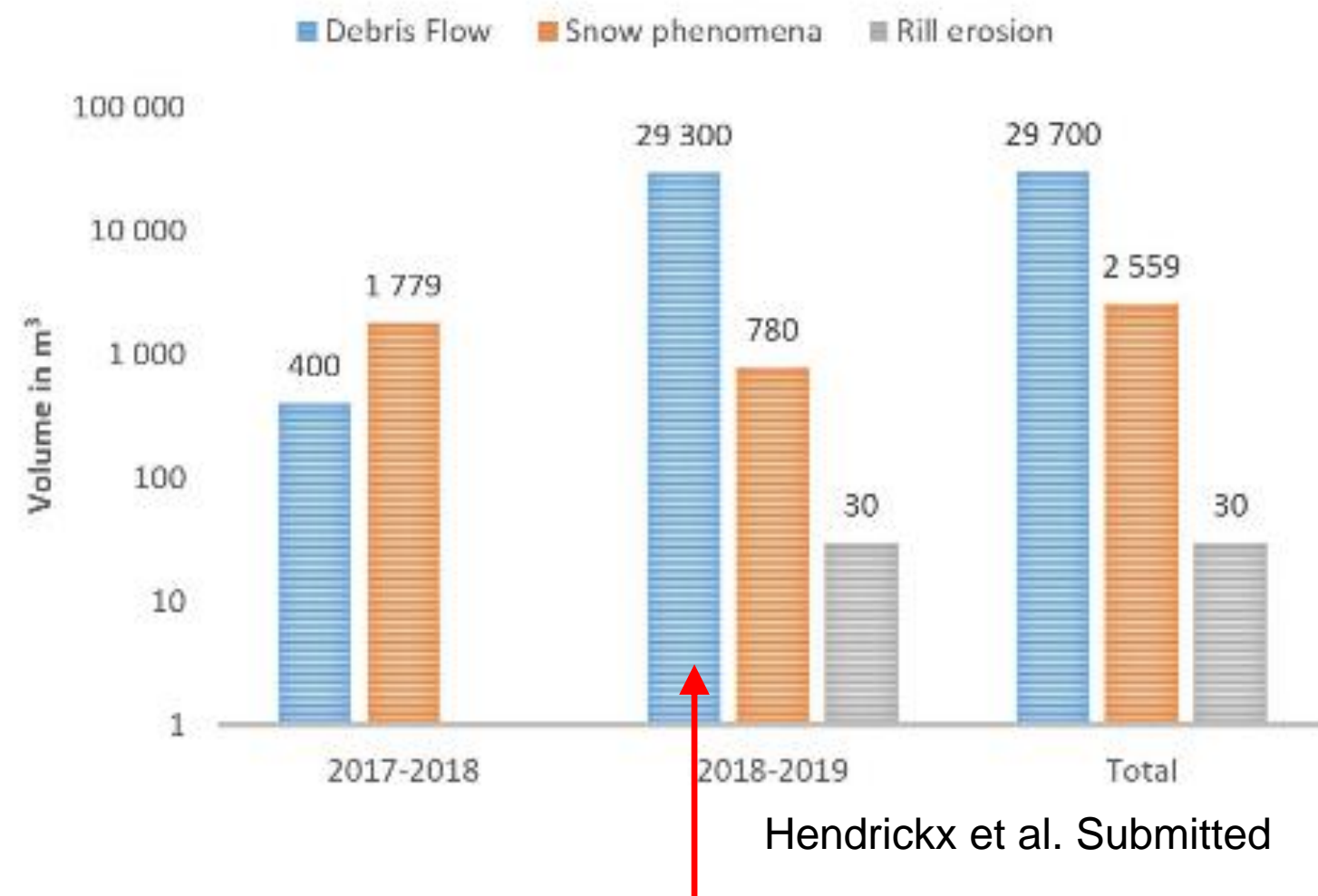


Figure 8. Talus slope geomorphology shown by the 10 cm resolution hill-shade and orthophoto derived from the UAV data of 2019, a) debris flow deposit, b) arched snow creep ridges, c) boulder pushed by slide/creep of the snow pack, here named as snow creep flutes, d) rill erosion in the more fine grained parts of the talus slope.

CASE STUDY 2: COL DU SANETSCH TALUS SLOPE

Figure 9. Volumes per main geomorphic reworking process per year on a logarithmic scale.



Very large debris flow event
in 2019

- Annual sediment rates consist of debris flow channel erosion and fill (~10 – 100 m³ per channel) and material displaced by snow creep/push (~1,000 – 2,000 m³) (Fig. 9) and are the most important sediment redistribution actor on the talus slope in years when no debris flow activity is observed

CASE STUDY 2: COL DU SANETSCH TALUS SLOPE

Hendrickx et al. Submitted

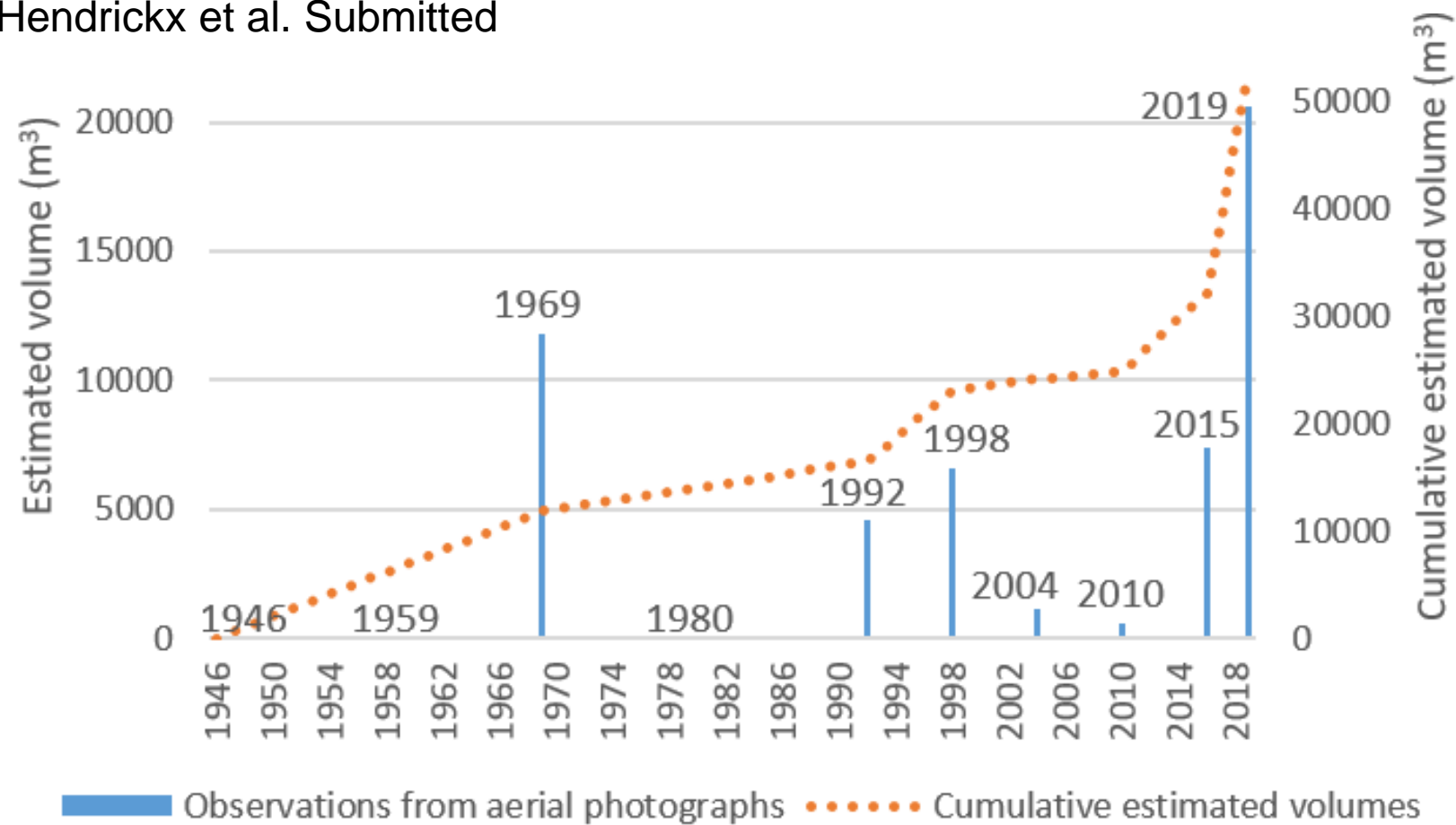


Figure 9. The estimated debris flow volume for the different time periods, based on historical aerial photographs dating back until 1946 (see examples at the end of the slides)

- In 2019, the largest debris flow event in the last 70 years was observed (Fig. 9), with a displaced volume $> 20,000 \text{ m}^3$.
- Most of the mobilized sediments originated from incision of the talus apex area, while only a small part came from intermediate debris storage within rock wall couloirs.

CASE STUDY 2: COL DU SANETSCH TALUS SLOPE

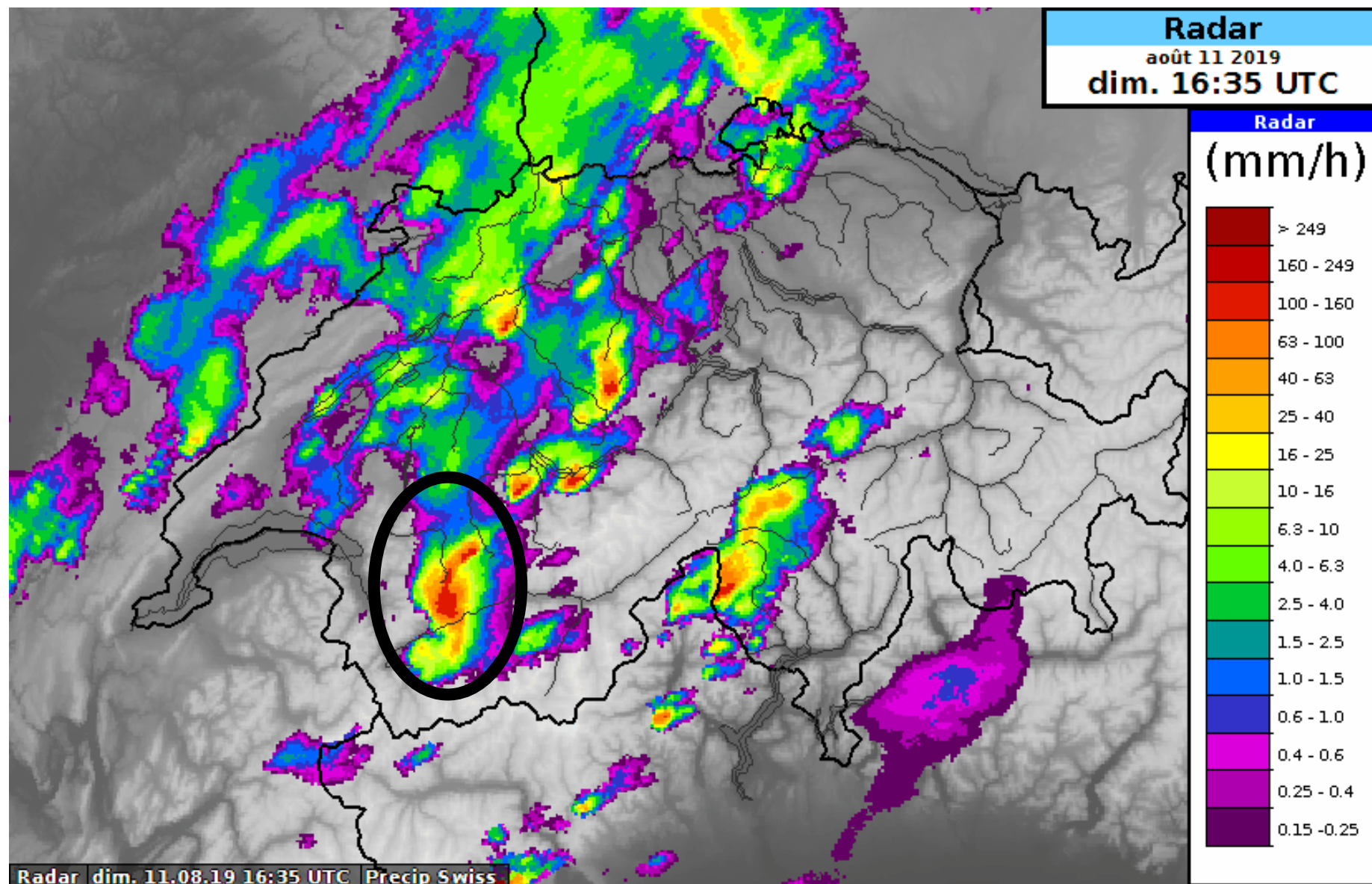


Figure 10. Radar data on August 11, 2019

- This debris flow event is linked to an intense prefrontal thunderstorm, causing a rainfall intensity of almost 10 mm/10 min for the study area (Fig. 10) (MeteoSwiss station VSTSN, 3 km from the study area).
- Future climate predictions show an increase in these events in the region, potentially altering the debris flow frequency and the dominant geomorphic process active on such slopes.

CONCLUSION

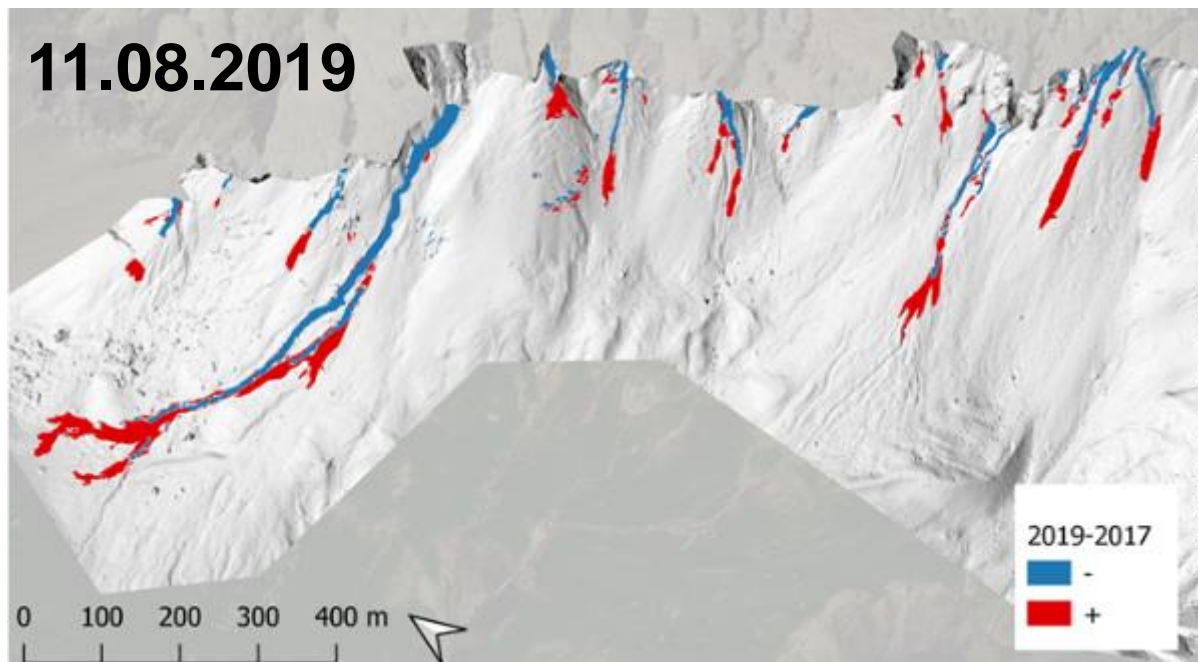
PRELIMINARY CONCLUSIONS

28.08.2019



In a time-span of 3 yrs we observed the destabilization and the failure of an entire rock face. Permafrost was present, but it remains unclear if its degradation is an explanatory factor, rather than a geological predisposition.

11.08.2019



Intense rain fall events have the potential to mobilise a lot of sediment in an otherwise relatively stable talus slope environment, dominated by snow push phenomena.

Hanne Hendrickx

Research and teaching assistant

DEPARTMENT OF GEOGRAPHY

E hanne.hendrickx@ugent.be


T +32 9 264 46 19

www.ugent.be

www.geoweb.ugent.be

 Geografie UGent

 @HendrickxHanne

 /Hanne_Hendrickx
Project: Talus slope dynamics in a permafrost environment

 Sketchfab/hannehendrickx

APPENDIX

MEASURING EQUIPMENT GROSSE GRABE



- Long range Riegl-V6000
- Scanning from a distance of ~ 1 km
- Accuracy: 3 cm (after coarse and fine (MSA) co-registration in RiScanPro based on stable areas)
- Resolution: downscaled to 10 cm using an octree filter

MEASURING EQUIPMENT COL DU SANETSCH

Hendrickx et al. Submitted

	Hexacopter DJI F550	DJI Phantom 4 pro
Camera :	Panasonic Lumix DMX-GM5	Integrated
	Zoom lens	Prime lens
Sensor size (pixels)	4592 x 3448	5472 x 3648
Sensor size (mm)	17.3 x 13	13.2 x 8.8
Aperture	Varied	F/5.6 – 6.3
Shutter speed (s)	> 1/500	1/200 – 1/800
Shutter type	Global	Global
ISO	400	100
Focal length (mm)	12-20	8.8

Table A1. Characteristics of Uncrewed Aerial Vehicle (UAVs) cameras used in this study

Hendrickx et al. Submitted

	2017	2018	2019
Used UAV	Hexacopter DJI F550	Hexacopter DJI F550	DJI Phantom 4 Pro
Flight planning software	Mission Planner	Mission Planner	UgCS
Number of flights	18	25	15
Survey days	4	3	3
Covered area in km²	1.2	1.3	2.0
GSD in cm/pixel	3.5 – 5.3	3.5 – 5.3	2.0
Used dGNNS system	Trimble RTK v4	Leica RTK GPS	Leica RTK GPS
Number of GCPs (& CPs)	10(4)	20(6)	24(15)

Table A2. Characteristics of the survey data for the three years



DATA PROCESSING COL DU SANETSCH

Hendrickx et al. Submitted

Hendrickx et al. Submitted

	Registration error (RMSE on 25 CPs)	LoD _{95%}	LoD _{80%}
UAV $\sigma_{\text{seperate alignment}}$	0.120	0.273	0.178
UAV $\sigma_{\text{co-alignment}}$	0.071	0.196	0.128
TLS σ	0.023	0.065	0.042

Table A3. Registration error (RMSE) per 3D model and the calculated level of detections in m. UAV = Uncrewed Aerial Vehicle, TLS = Terrestrial Laser Scanner, LoD = Level Of Detection

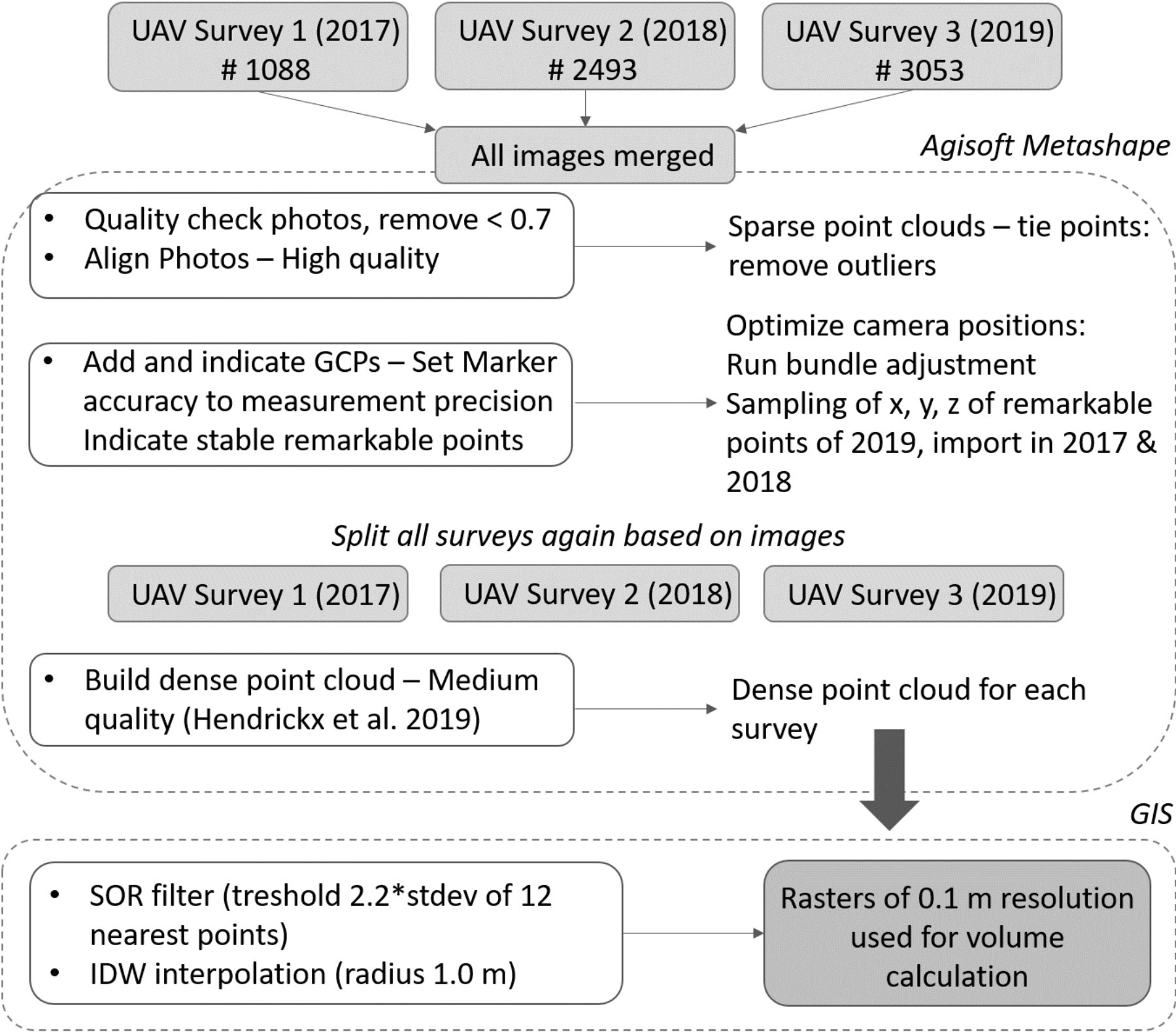


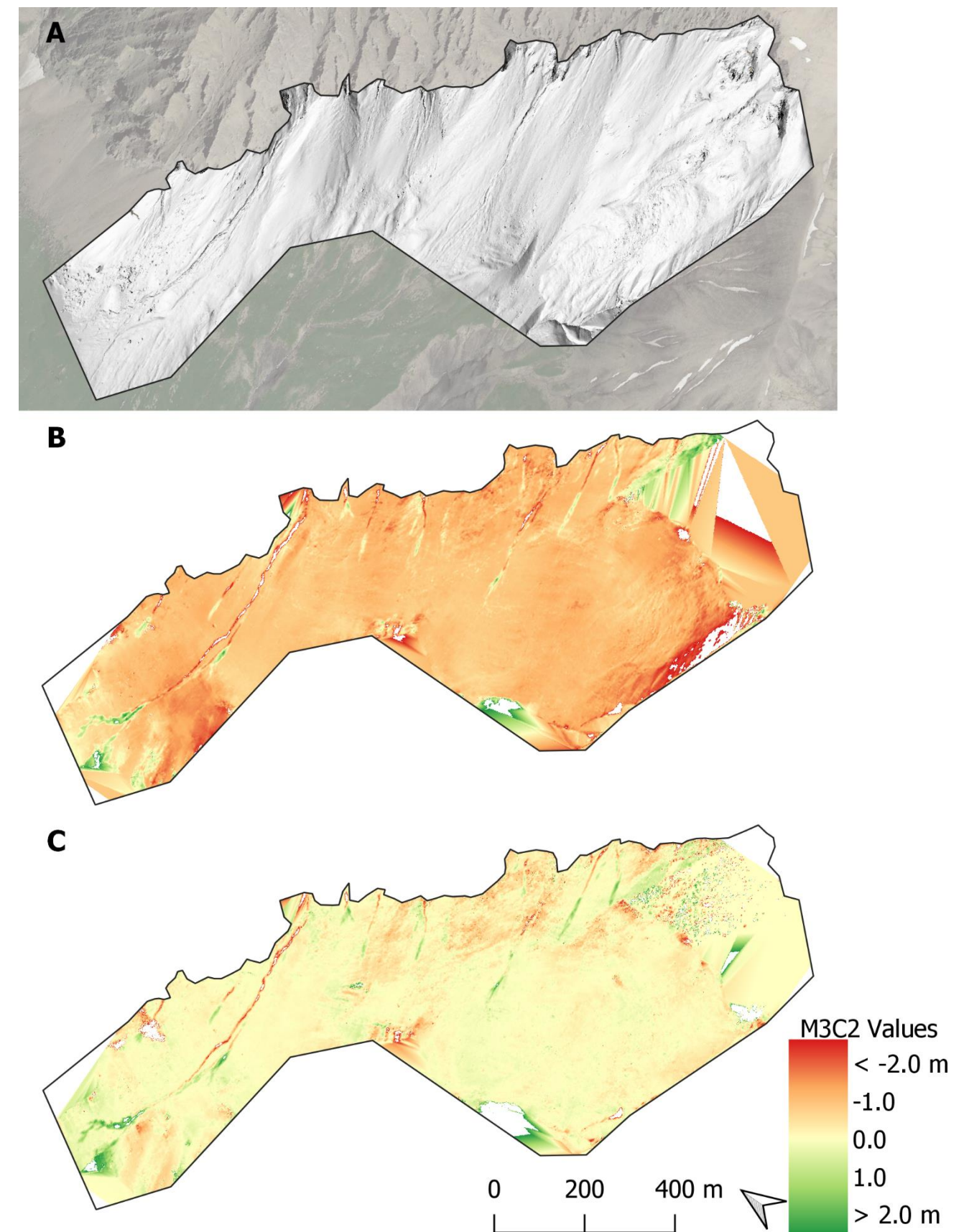
Fig A1. Workflow in Metashape and GIS environment, adopting co-alignment methodology (Cook & Dietze, 2019).

DATA PROCESSING COL DU SANETSCH

UAV data is prone to deformations, especially if the ground control points (GCPs) are not evenly distributed. We confirm that the co-alignment approach (Cook & Dietze, 2019)* is useful to improve the comparative accuracy when GCPs do not have an optimal spatial distribution.

*Also view EGU abstract EGU2020-11735 from the same authors in the session G11.3 and GM2.3

Fig A2. a) hillshade of the study area, b) deformations adopting standard Methashape workflow, c) deformations adopting the co-alignment approach



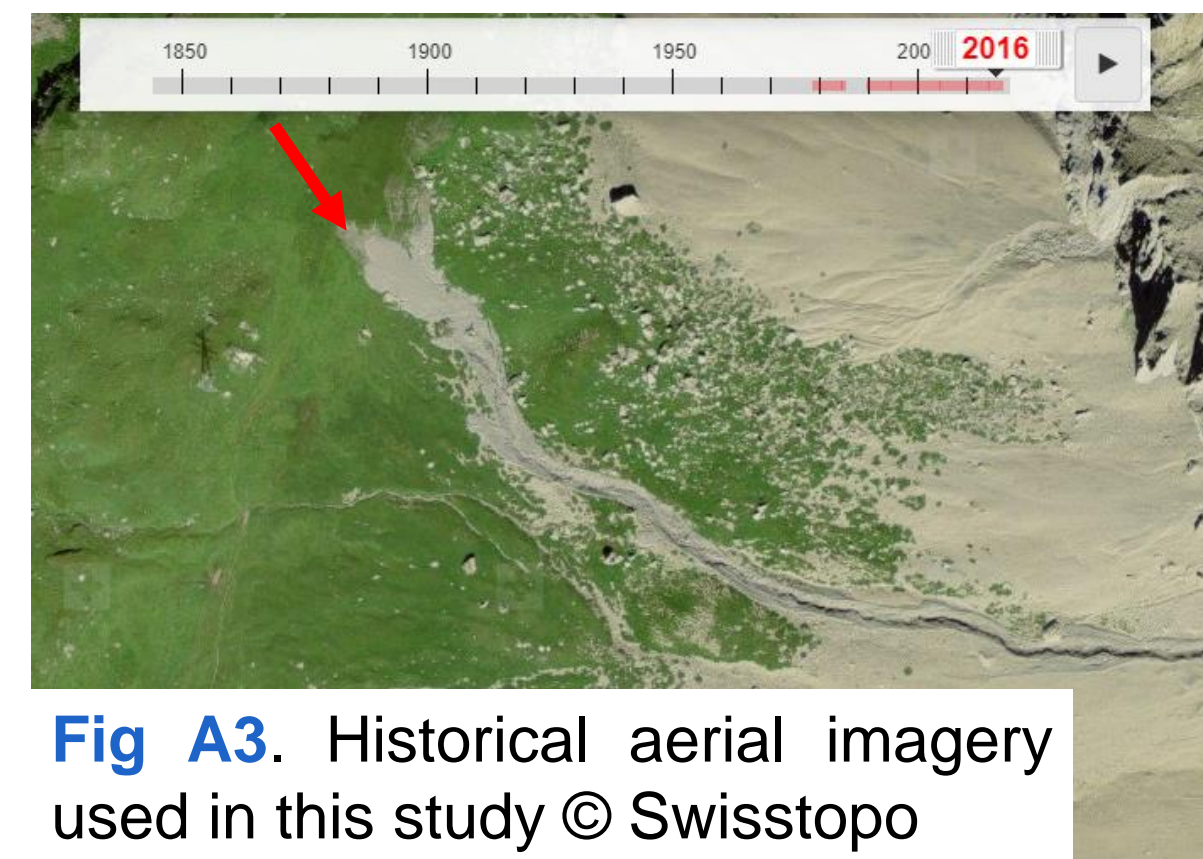
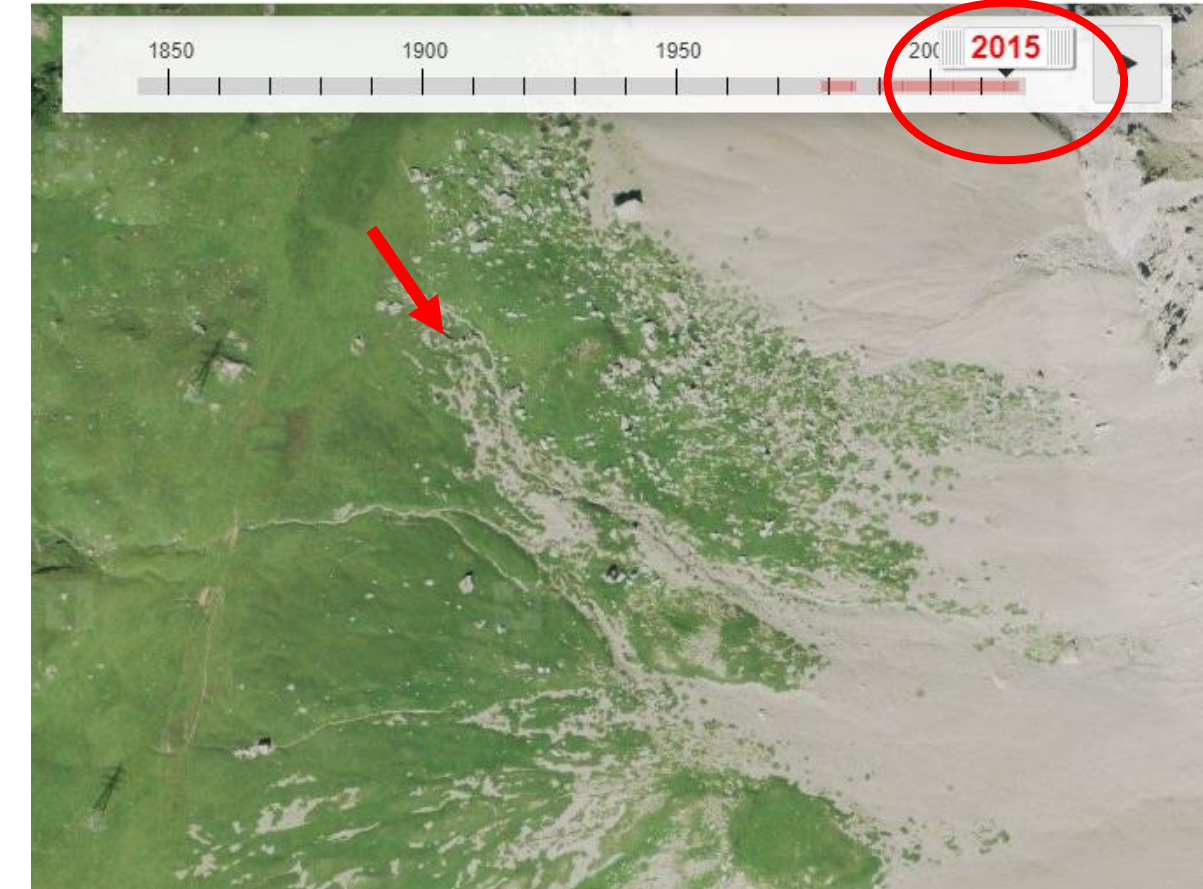
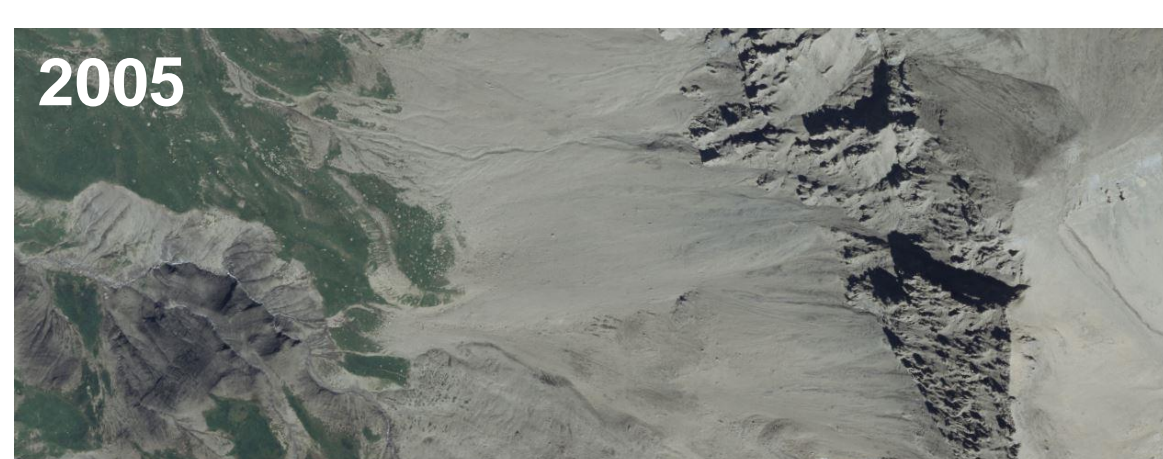
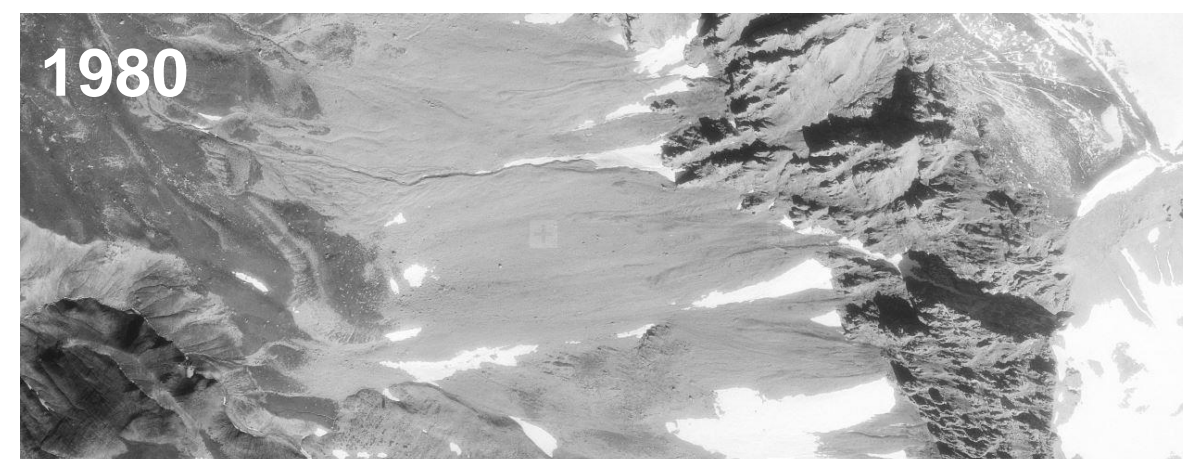
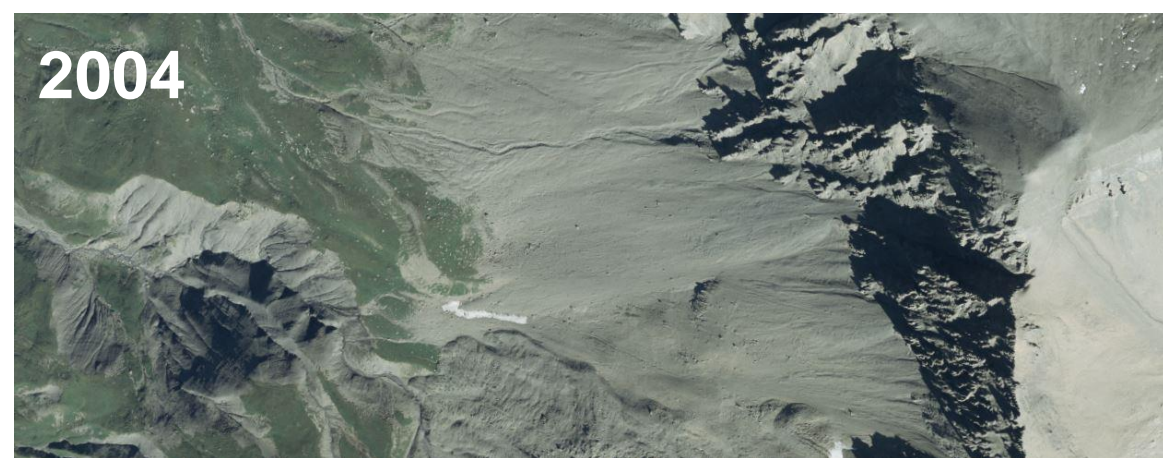
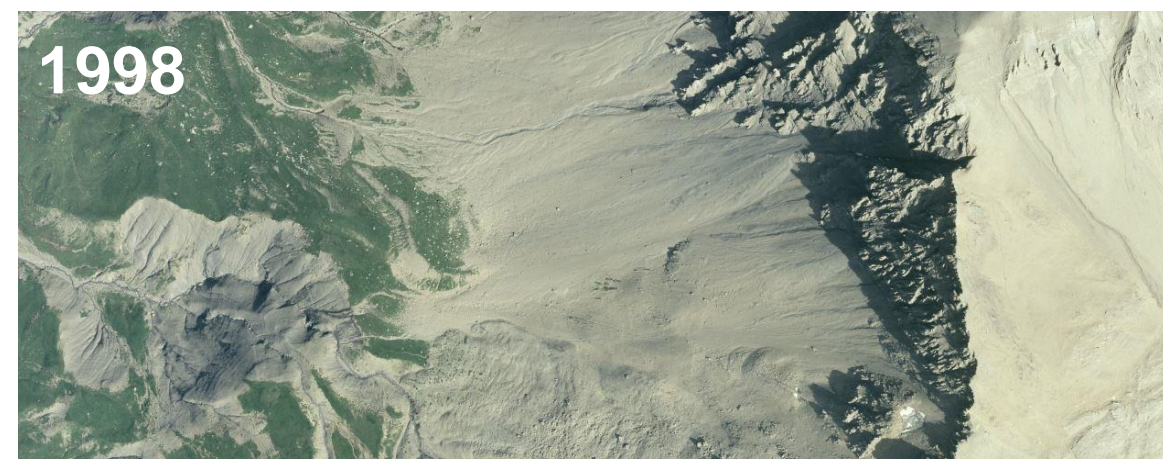
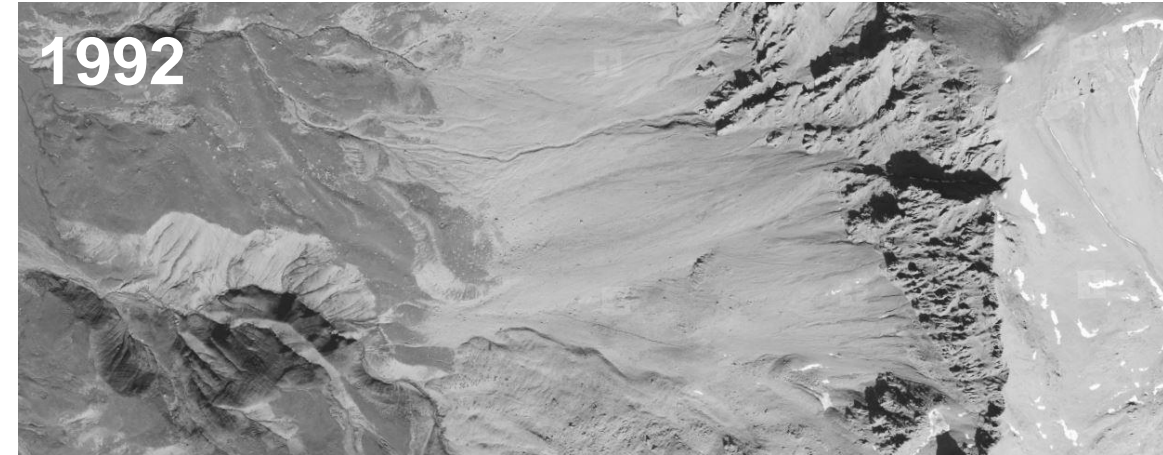
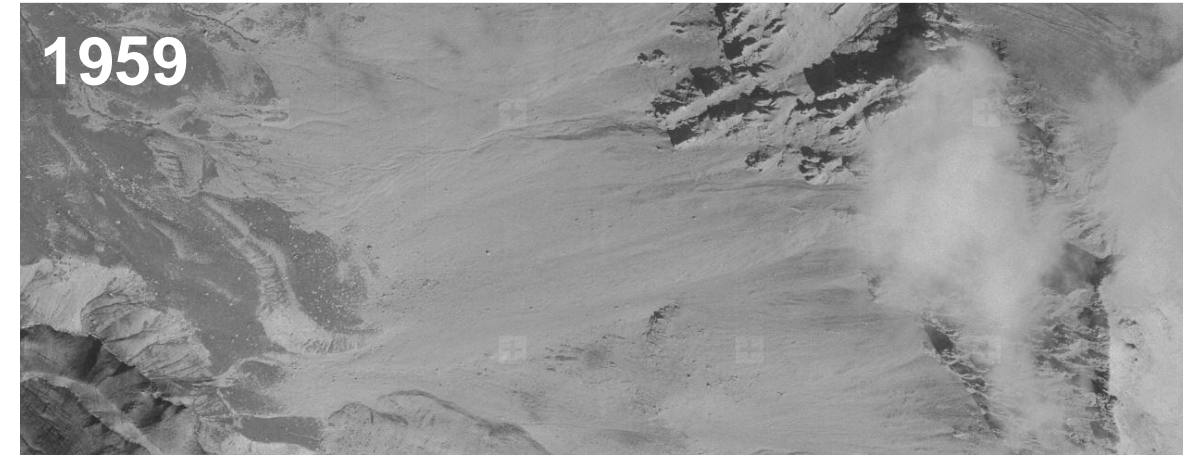


Fig A3. Historical aerial imagery used in this study © Swisstopo